Assessment of Gel Formation in Colloidal Dispersions during Mixing in Turbulent Jets

Miroslav Soos
Dept. of Chemistry and Applied Biosciences, Institute for Chemical and Bioengineering, ETH Zurich, 8093 Zurich, Switzerland

Daniele L. Marchisio
Dip. di Scienza Applicata e Tecnologia, Istituto di Ingegneria Chimica, Politecnico di Torino, C.so Duca degli Abruzzi 24, I-10129 Torino, Italy

Jan Sefcik
Dept. of Chemical and Process Engineering, University of Strathclyde, James Weir Building, 75 Montrose Street, Glasgow G1 1XJ, Scotland, UK

DOI 10.1002/aic.14268
Published online October 28, 2013 in Wiley Online Library (wileyonlinelibrary.com)

Onset of gel formation upon mixing between colloidal dispersions and coagulant solutions in turbulent jets was studied using a combination of computational fluid dynamics (CFD) and population balance equation (PBE). To describe the interaction between turbulence fluctuations and particle aggregation, a micromixing model based on presumed probability density function was implemented inside the CFD code. Furthermore, effect of the solid phase on the fluid flow was modeled through an effective viscosity of the mixture evaluated from PBE. The results are presented in the parameter space of the primary particle diameter and the solid volume fraction where strong interplay between mixing and aggregation mechanisms controls the gelation phenomena and consequently also the fluid dynamics. Simulation results are in good agreement with observations from gelation experiments of concentrated nanoparticle suspensions injected into coagulant solutions. © 2013 American Institute of Chemical Engineers *AIChE J*, 59: 4567–4581, 2013
Keywords: aggregation, gelation, turbulent flow, mixing, micromixing, colloidal dispersion

Introduction

Processing of colloidal dispersions is an important step in production of particulate materials in numerous industrial applications, for example, polymer processing, pigment manufacturing, waste water treatment and so forth. Because the typical sizes of primary colloidal particles are on the order of hundreds of nanometers, classical separation processes such as filtration or sedimentation for removal of solid particles from the carrier liquid are not straightforward and challenging to implement. A convenient alternative is to induce particle aggregation, resulting in size enlargement, where aggregates with size of hundreds of microns can be obtained and can be easily separated from the liquid phase by filtration.

Commonly, colloidal particles are stabilized by ionic and/or nonionic (steric) surfactants adsorbed on their surface.[1] While in the case of steric surfactants, colloidal stability is not reduced by adding electrolyte coagulants, in the case of ionic surfactants addition of salts to increase ionic strength reduces repulsive forces so that particles can be brought into close proximity, enabling van der Waals attraction forces to overcome repulsion, and therefore leading to particle aggregation. There are several mechanisms which can cause particle collision, such as Brownian motion, mean velocity gradients, or turbulent fluctuations. To study these mechanisms, very low solid volume fractions of primary particles are commonly used.[2–7] Under such conditions, complete mixing of stable particle dispersions with coagulant solutions is typically much faster than the time scale of aggregation. In contrast, industrial applications deal with rather high particle concentrations, commonly greater than 10 wt%, resulting in characteristic aggregation times being comparable or even shorter than that of mixing.[8] In fact, as was shown by Vaccaro et al.[8] important aspects which significantly influence the morphology of the final product include the way in which the two streams are mixed and the concentration of the primary particles. As pointed out by these authors to quantitatively describe process of gelation would require coupling population balance model with computational fluid dynamics (CFD) and suitable micromixing model. Furthermore, viscosity increase due to aggregation should be included to introduce the effect of produced clusters on the fluid flow. Even though the effect of mixing on fast processes, such as combustion or nanoparticle precipitation, was studied in the literature,[9–13] relevant theoretical concepts have not been previously applied to study the process of aggregation of concentrated colloidal dispersions.

Therefore, the aim of this work is to develop such a model and consequently to investigate, from the computational

Additional Supporting Information may be found in the online version of this article.

Correspondence concerning this article should be addressed to M. Soos at miroslav.soos@chem.ethz.ch.

point of view, the interaction between mixing and aggregation by means of a combination of population balance equation (PBE) and CFD.[14] To study effects of mixing on the aggregation process, simulations were carried out in a concentric tubular geometry allowing application of steady state assumptions. The PBE was solved by the quadrature method of moments (QMOM) and was implemented in a commercial CFD code ANSYS FLUENT v12. Since aggregation can be very fast, a micromixing model to describe the interaction between particle aggregation and turbulent fluctuations (averaged out by applying Reynolds-Average Navier-Stokes) based on a presumed probability density function (PDF) method was solved simultaneously with PBE inside the CFD code. The internal morphology of the produced aggregates was incorporated in the model using a fractal scaling approach and results were obtained for different values of the fractal dimension, that is, d_f equal to 1.8 and 2.2 characterizing fully and partially destabilized conditions. Because our goal is to describe the early stage of the mixing between two streams containing particles and coagulant, simulations were restricted to pure aggregation neglecting breakage. This is justified for systems where aggregates do not become large enough to be subject to hydrodynamic breakage[15–17] within the range of conditions investigated. As the aggregates grow their effect on the surrounding fluid starts to be important and this was taken into account by introducing an effective viscosity of the solid–liquid mixture evaluated from the local value of the occupied volume fraction. Properties of the distribution of aggregates were studied in terms of the mean radius of gyration and the occupied volume fraction.

Model Description

Population balance equation

The evolution of the particle-size distribution (PSD) due to the aggregation of monodisperse primary particles in space can be described by the PBE

$$\frac{\partial n(\omega;\mathbf{x},t)}{\partial t}+\frac{\partial}{\partial x_i}\left[\langle u_i\rangle n(\omega;\mathbf{x},t)\right]-\frac{\partial}{\partial x_i}\left(D_t\frac{\partial n(\omega;\mathbf{x},t)}{\partial x_i}\right)$$
$$=+\frac{1}{2}\int_0^{\xi}K^A(\omega-\omega',\omega')n(\omega-\omega';\mathbf{x},t)n(\omega';\mathbf{x},t)d\omega' \quad (1)$$
$$-n(\omega;\mathbf{x},t)\int_0^{\infty}K^A(\omega,\omega')n(\omega';\mathbf{x},t)d\omega'$$

where $n(\omega;\mathbf{x},t)$ is the Reynolds-averaged PSD, ω is the dimensionless mass of an aggregate (expressed in term of the number of primary particles), $\mathbf{x}$ is the spatial coordinate vector, t is physical time, $\langle u_i\rangle$ is the Reynolds-averaged fluid velocity in the i-th spatial direction, D_t is the turbulent diffusivity, and $K^A(\omega,\omega')$ is the aggregation kernel of two aggregates with masses ω and ω'. It is worth noting that last mentioned strongly depends on the local shear rate (see below). Particle turbulent diffusivity was assumed to be identical to that of the fluid and using standard modeling assumption, results in

$$D_t=\frac{C_\mu k^2}{\mathrm{Sc}_t\varepsilon} \quad (2)$$

where k is the turbulent kinetic energy, ε is the turbulent dissipation rate, Sc_t is turbulent Schmidt number (usually assumed to be equal to 0.7) and C_μ is a parameter equal to 0.09. It is clear that to solve the PBM reported in Eq. 1, a detailed knowledge of the flow field to evaluate turbulent properties described in Eq. 2 and aggregation kernel $K^A(\omega-\omega',\omega')$ is needed. For this reason, the PBE needs to be coupled with mass and momentum balance equations with appropriate closure for the velocity fluctuations.

Micromixing model

The PBE Eq. 1 was derived under the hypothesis that the time-scale of mixing due to turbulence fluctuations is well separated from the characteristic time-scale of aggregation. This hypothesis does not hold anymore under very high solid volume fractions. In fact, under these operating conditions aggregation of colloidal particles is very fast, and local fluctuations can heavily affect the overall aggregation rate.

The process under investigation involves mixing of two inlet streams: the stable colloidal dispersion and the coagulant solution. When modeling mixing processes it is useful to define a nonreacting scalar, namely the mixture fraction $\xi(\mathbf{x},t)$, that quantifies the amount of fluid coming from one inlet (e.g., inlet 1) with respect to the other one (e.g., inlet 2).[18] For example, when two streams with volumetric flow rates equal to Q_1 and Q_2 are mixed, the complete mixing condition is verified when the mixture fraction is equal to the following quantity (assuming no volume change upon mixing)

$$\overline{\xi}=\frac{Q_1}{Q_1+Q_2} \quad (3)$$

Because in a turbulent system, all quantities (including the mixture fraction) are subjected to fluctuations, the concept of Reynolds averaging is introduced and the Reynolds-averaged mixture fraction is usually denoted by $\langle\xi\rangle$. Therefore under turbulent conditions, the system is perfectly macromixed when the local value of the Reynolds-averaged mixture fraction is equal to the volume-averaged one $\langle\xi\rangle=\overline{\xi}$.

This condition, however, does not specify the state of the fluid at the microscale level. The fluid is said to be micromixed when the mixture fraction variance, denoted as $\langle\xi'^2\rangle$, is equal to zero and therefore the local values of the mixture fraction are equal to its Reynolds-averaged value $\xi=\langle\xi\rangle$.

In order to describe turbulent fluctuations and their interaction with the PBE, the PDF approach was used. With this approach, turbulence fluctuations are described in terms of a PDF whose functional form is assumed *a priori*. In this work, the PDF is assumed to be constituted by a summation of N delta functions and each delta function can be thought of as an environment. If the mixture fraction is the only scalar involved, the PDF becomes as follows[18]

$$f_\xi(\psi;\mathbf{x},t)\equiv\sum_{n=1}^{N_e}p_n(\mathbf{x},t)\delta[\psi-\xi_n(\mathbf{x},t)] \quad (4)$$

where $p_n(\mathbf{x},t)$ is the probability of mode n or the volume fraction of environment n, $\xi_n(\mathbf{x},t)$ is the value of the mixture fraction corresponding to mode n or the local value of the mixture fraction in environment n, ψ is the composition vector characterizing the final mixture, and N_e is the total number of modes/environments.

From Eq. 4, the averaged value of the mixture fraction is given by

$$\langle \xi \rangle = \sum_{n=1}^{N_e} p_n \xi_n \tag{5}$$

Whereas, the mixture fraction variance is defined as

$$\langle \xi'^2 \rangle = \sum_{n=1}^{N_e} p_n \xi_n^2 - \langle \xi \rangle^2 \tag{6}$$

In this work, the presumed PDF method is applied by using three modes ($N_e=3$) corresponding to three environments. Similar to the experimental setup of Vaccaro et al.,[8] it is assumed that the stream of a dispersion of stable primary particles enters the reactor through mode/environment 2, whereas the stream of coagulant solution is fed through the other one (i.e., mode/environment 1). Therefore, coagulation does not occur in the two feeding modes/environments, and in fact the mixture fraction in these modes/environments (i.e., ξ_1 and ξ_2) stay constant and equal to the inlet values, while aggregation occurs only in mode/environment 3 that is formed when modes/environments 1 and 2 are micromixed. Details concerning this method, known as finite-mode PDF model, can be found in literature.[18]

In the final form of the model, the transport equations for probabilities/volume fractions of modes/environments 1 and 2 are solved

$$\begin{aligned} &\frac{\partial p_1}{\partial t} + \frac{\partial}{\partial x_i}[\langle u_i \rangle p_1] - \frac{\partial}{\partial x_i}\left(D_t \frac{\partial p_1}{\partial x_i}\right) \\ &= -\gamma p_1(1-p_1) + D_t \frac{2}{1-2\xi_3(1-\xi_3)}\left(p_3 \frac{\partial \xi_3}{\partial x_i}\frac{\partial \xi_3}{\partial x_i}\right) \end{aligned} \tag{7}$$

$$\begin{aligned} &\frac{\partial p_2}{\partial t} + \frac{\partial}{\partial x_i}[\langle u_i \rangle p_2] - \frac{\partial}{\partial x_i}\left(D_t \frac{\partial p_2}{\partial x_i}\right) \\ &= -\gamma p_2(1-p_2) + D_t \frac{2}{1-2\xi_3(1-\xi_3)}\left(p_3 \frac{\partial \xi_3}{\partial x_i}\frac{\partial \xi_3}{\partial x_i}\right) \end{aligned} \tag{8}$$

whereas the probability/volume fraction of mode/environment 3 is calculated through the following algebraic equation

$$p_3 = 1 - p_1 - p_2 \tag{9}$$

The mixture fraction values in modes/environments 1 and 2 are not calculated as they are constant and equal to their initial values, whereas the mixture fraction value in mode/environment 3 is given by the following equation

$$\begin{aligned} &\frac{\partial (p_3\xi_3)}{\partial t} + \frac{\partial}{\partial x_i}[\langle u_i \rangle (p_3\xi_3)] - \frac{\partial}{\partial x_i}\left(D_t \frac{\partial (p_3\xi_3)}{\partial x_i}\right) \\ &= +\gamma p_1(1-p_1)\xi_1 + \gamma p_2(1-p_2)\xi_2 - D_t \frac{2(\xi_1+\xi_2)}{1-2\xi_3(1-\xi_3)}\left(p_3 \frac{\partial \xi_3}{\partial x_i}\frac{\partial \xi_3}{\partial x_i}\right) \end{aligned} \tag{10}$$

where γ is now calculated as follows

$$\gamma = C_\phi \frac{\varepsilon}{k} \frac{\langle \xi'^2 \rangle}{\left[p_1(1-p_1)\left(1-\langle \xi \rangle_3\right)^2 + p_2(1-p_2)\langle \xi \rangle_3^2\right]} \tag{11}$$

The constant C_ϕ is usually assumed to be equal to 2 for fully developed turbulent flows. However, in order to account for the not completely developed shape of the scalar turbulence spectrum, C_ϕ can be calculated as a function of the local Reynolds number $\mathrm{Re}_1 = k/\sqrt{\varepsilon v}$ resulting in the following expression[19]

$$C_\phi(\mathrm{Re}_1) = A_2 + \frac{A_1 - A_2}{1 + {}^{\mathrm{Re}_1}/_{\mathrm{Re}_c}} \tag{12}$$

with $A_1=0.055$, $A_2=2.23$, $\mathrm{Re}_c=5.6$ (see Supporting Information Figure S1). The micromixing model is then coupled with the PBE, whose solution is discussed in the following paragraph.

Population balance model

As reported by Ramkrishna,[20] the PBE can be solved by using several approaches. Because the aim of this work is to numerically investigate aggregation under nonhomogeneous flow conditions, the PBE was solved inside the CFD code. Among the many available, the most convenient method to approach this problem is to make use of the method of moments.[21,22] This method simply consists of solving the transport equations for the moments of the PSD instead of the original PBE.[23] Consequently, the moment of order k of the PSD is defined as

$$\mu^k(\mathbf{x}, t) = \int_0^{+\infty} n(\omega; \mathbf{x}, t)\omega^k d\omega \tag{13}$$

As it has been reported before this equation must be solved in the CFD code and coupled with the micromixing model. Due to small size of primary particles as well as initial aggregates resulting in their Stokes number below one the fluid flow was modeled on a basis of a pseudohomogeneous dispersion. Under these conditions, the moments of the PSD will also be subjected to turbulent fluctuations, and therefore, they must be included as variables of the joint-composition PDF. As for the mixture fraction also moments will be defined in each mode/environment, and for example, with $\mu_n^k(\mathbf{x}, t)$ we denote the moment of the PSD of order k in mode/environment n.

Once the moment transform is applied to the original PBE, a closure problem is generated, in fact, some transport equations cannot be written explicitly in terms of the moments themselves. In order to overcome this problem, a quadrature approximation[24] is used, where any integral involving the PSD is expressed in terms of the weights and abscissas of the quadrature approximation. For example, the k-th moment in mode/environment n can be written in terms of a quadrature approximation of order N as follows

$$\mu_n^k(\mathbf{x}, t) \approx \sum_{i=1}^{N} w_{i,n}\omega_{i,n}^k \tag{14}$$

where $w_{i,n}$ are the weights and $\omega_{i,n}$ are the abscissas of the quadrature approximation in mode/environment n. As it is possible to show, the nodes of the quadrature approximation of order N are the zeros of the polynomial of the same order orthogonal to the PSD, and they can be calculated by knowing the first $2N$ moments of the PSD. The product-difference (PD) algorithm[25] is used here to evaluate the weights and abscissas of the quadrature approximation from the moments based on the calculation of the eigenvalues and eigenvectors of a small tridiagonal matrix of rank N. The number of nodes in QMOM used in this simulation was equal to 3.

Finally, after applying the quadrature approximation (Eq. 14) and after implementing the micromixing model with three modes/environments ($N_e=3$), the transport equation for

the moment of order k in mode/environment 3 (Eq. 10) becomes

$$\frac{\partial\left(p_3\mu_3^k\right)}{\partial t}+\frac{\partial}{\partial x_i}\left[\langle u_i\rangle\mu_k\left(p_3\mu_3^k\right)\right]-\frac{\partial}{\partial x_i}\left(D_{\mathrm{t}}\frac{\partial\left(p_3\mu_3^k\right)}{\partial x_i}\right)$$
$$=\gamma p_1(1-p_1)\left(\phi v_p^{k-1}\right)-D_{\mathrm{t}}\frac{2(\xi_1+\xi_2)}{1-2\xi_3(1-\xi_3)}\left(p_3\frac{\partial\xi_3}{\partial x_i}\frac{\partial\xi_3}{\partial x_i}\right)\left(\phi v_p^{k-1}\right)$$
$$+p_3\left\{\frac{1}{2}\sum_{i=1}^{N}\sum_{j=1}^{N}\left[\left(\omega_{i,3}+\omega_{j,3}\right)^k-\omega_{i,3}^k-\omega_{j,3}^k\right]K^A\left(\omega_{i,3},\omega_{j,3}\right)w_{i,3}w_{j,3}\right\} \tag{15}$$

where the correction, that is, second term on the right hand side, is calculated through the mixture fraction. It is worth noting that transport equations for moments in modes/environments 1 and 2 are not solved as their values are constant and equal to those of the inlet, that is, $\mu_1^k=0$ and $\mu_2^k=\phi v_p^{k-1}$.

Aggregation kernel

Because the objective of this work is to investigate particle gelation of concentrated colloidal suspensions under heterogeneous flow conditions, only aggregation will be considered here. Aggregation is driven by several mechanisms, such as Brownian motions and fluid velocity gradients, including mean velocity gradients in laminar flows, velocity fluctuations in turbulent flows, or velocity gradients created by differential settling during sedimentation. Typically under turbulent conditions, the contribution of sedimentation can be neglected, and assuming fully destabilized colloidal particles, the aggregation rate constant can be expressed as the sum of two contributions, one due to Brownian motion and another one due to turbulent fluctuations[26]

$$K^{\mathrm{A}}(\omega-\omega',\omega')=K^{\mathrm{Brownian}}_{\omega-\omega',\omega'}+K^{\mathrm{Shear}}_{\omega-\omega',\omega'} \tag{16}$$

Brownian aggregation is driven by collisions of particles due to their Brownian motion and becomes particularly important for submicron particles, where the corresponding rate constant is given by[27]

$$K^{\mathrm{Brownian}}_{\omega-\omega',\omega'}=\frac{4\pi}{W}\left(D_{\omega-\omega'}+D_{\omega'}\right)\left(R_{c,\omega-\omega'}+R_{c,\omega'}\right) \tag{17}$$

where W is the Fuchs stability ratio which depends on the interaction forces between colliding aggregates, $D_{\omega-\omega'}$ and $D_{\omega'}$ are their diffusion coefficients that depend on their size (see below), while $R_{c,\omega-\omega'}$ and $R_{c,\omega'}$ are their collision radii.

Shear aggregation is driven by collision of particles due to spatial fluid velocity gradients and the corresponding rate constant can be expressed as follows[27]

$$K^{\mathrm{Shear}}_{\omega-\omega',\omega'}=\alpha_A G\left(R_{c,\omega-\omega'}+R_{c,\omega'}\right)^3 \tag{18}$$

where α_{A} is the aggregation rate prefactor which dependents on particle interactions and the surrounding flow field and here it is chosen to be equal to 1.3,[28] G is the shear rate (see Eq. 19). Based on the work of Saffman and Turner,[28] under turbulent conditions, the shear rate can be calculated as follows

$$G(\mathbf{x})=\sqrt{\frac{\varepsilon}{v}} \tag{19}$$

where v is the kinematic viscosity.

Aforementioned, aggregation rate constants for Brownian motion and shear aggregation (Eqs. 17, 18) are valid only for fully destabilized conditions, that is, when there is no electrostatic repulsion between aggregating objects, also known as diffusion limited cluster–cluster aggregation (DLCA) regime. Conversely, when partial destabilization of aggregating particles is considered, also known as reaction limited aggregation cluster–cluster aggregation regime, the rate of aggregation decreases exponentially with the energy barrier between aggregating objects resulting in much longer aggregation times. Because the process of mixing between stable colloidal dispersion and coagulant solution considered here is rather fast, typically being completed within a fraction of a second, in what follows we consider that aggregation occurs only in the DLCA regime once particles become mixed with a coagulant. In order to account for the extent of mixing on the real aggregation rate constant, and therefore, to reduce the rate of aggregation immediately after latex entering the domain, aggregation rate constant is calculated as a product of the rate constant corresponding to the DLCA regime (Eqs. 17, 18) and the probability of environment 3 calculated by micromixing model discussed earlier (Eq. 9).

Structure of aggregates

Equation 1 is a balance written in terms of the PSD $n(\omega;\mathbf{x},t)$ that is expressed in terms of the dimensionless mass of the colliding clusters. Conversely, the aggregation kernel $K^A(\omega-\omega',\omega')$ is a function of collision radii of two aggregating clusters, so appropriate relationships are required to relate mass and size of the clusters. In the case of colloidal systems, it is well known that aggregates constituted by a large number of primary particles, form randomly shaped clusters that can be described by a fractal scaling relationship between the dimensionless mass ω and its radius of gyration $R_{g,\omega}$[29]

$$\omega=k_{\mathrm{g}}\left(\frac{R_{\mathrm{g},\omega}}{R_{\mathrm{P}}}\right)^{d_{\mathrm{f}}} \tag{20}$$

where R_{p} is the radius of the primary particles, k_{g} is a scaling prefactor of the order of unity, and d_{f} is the fractal dimension. As was shown by Lattuada et al.,[30,31] a similar relationship is also valid for the collision radius $R_{c,\omega}$ and assuming scaling prefactor equal to unity, the following relationship is obtained:

$$R_{c,\omega}=R_P\omega^{1/d_{\mathrm{f}}} \tag{21}$$

In turn the diffusion coefficient D_ω, introduced in Eq. 17, can be calculated through the Stokes-Einstein equation, resulting in

$$D_\omega=\frac{k_{\mathrm{B}}T}{6\pi\eta}\frac{1}{R_{\mathrm{P}}}\omega^{-1/d_{\mathrm{f}}} \tag{22}$$

where k_{B} is the Boltzmann's constant, T is the absolute temperature, η is the dynamic viscosity of the fluid.

As it has been previously proposed,[32,33] the scaling prefactor in the definition of the collision radius can be considered effectively equal to unity, as it can be conveniently included in the kernel prefactors W and α_A, which anyway need to be extracted from fitting experimental data.

Effective viscosity of dispersion

As it was mentioned above, there is a direct coupling between fluid flow and aggregation process. In fact, the aggregation kernel is related to the turbulent energy

dissipation rate. Conversely, as the aggregates grow and occupy more and more space, they start interacting with the surrounding fluid by changing the local apparent viscosity. Based on the work of Krieger and Dougherty[34] and Quemada,[35] the apparent viscosity of a solid–liquid dispersion can be described in terms of the effective volume fraction, according to the following equation

$$\eta=\eta_0\left(1-\frac{\phi_{\text{eff}}}{\phi_{\text{m}}}\right)^{-q} \tag{23}$$

where η_0 is the dynamic viscosity of the pure liquid without solid particles, ϕ_{m} is the maximum packing volume fraction, ϕ_{eff} is the effective volume fraction of the particles in the mixture, and q is a scaling exponent. It is clear that the choice of the parameters in the Eq. 23 is system dependent.

As described in the literature,[36] in the case of monodisperse particles, the volume fraction is defined by the mass and density of the primary particles; whereas in the case of the fractal aggregates, the situation is more complicated. First of all, aggregate geometry does not follow standard Euclidean scaling ($\omega \propto R^3$), but its characteristic size increases faster than its mass so aggregates contain increasingly significant portion of voids occupied by the liquid. Second, because the aggregation leads to broadening of the cluster mass distribution (CMD), the population of aggregates cannot be approximated as monodisperse and instead the information about the whole distribution has to be incorporated. Therefore, to include these important features of fractal aggregates, the effective volume fraction ϕ_{eff} in Eq. 23 will be approximated by the volume fraction occupied by aggregates defined as

$$\phi_{\text{occ}}=\int_{\omega} n(\omega;\mathbf{x},t)V_{\omega}d\omega=\frac{4}{3}R_p^3\int_{\omega} n(\omega;\mathbf{x},t)\omega^{3/d_f}d\omega \tag{24}$$

As it was shown by Sandkühler et al.,[37,38] the occupied volume fraction can be efficiently used to determine the condition when aggregating clusters interconnect and form a network in the whole available volume and therefore can strongly affect the flow and turbulence fields in the coagulator.

Another important parameter appearing in the Eq. 23 is the value of the maximum packing fraction ϕ_{m} when viscosity diverges to infinity. This value can be found in the literature only for the dispersions of equally sized spheres assuming certain geometrical arrangement of the closed packing. The maximum packing fraction ranges from 0.524 to 0.74 for simple cubic and hexagonal close-packed arrangement, respectively, which is in good agreement with results of Sandkühler et al.[37,38] where gel formation under static conditions was observed when ϕ_{occ} reaches value around 0.5. Because all mentioned values are of a similar magnitude and because arrangement of the particles in the aggregate is close to random packing in what follows we will use the value of ϕ_{m} equal to 0.63 found by McGeary[39] from settling experiment. Moreover, this value is equal to the average of the interval mentioned earlier.

Last parameter in Eq. 23 which controls the increase of viscosity is the exponent q whose value according to several theoretical and experimental studies varies in the range from 1.3 to 2.0.[36,40–42] On one side, for dilute conditions viscosity needs to follow the Einstein's limit [43] where the relative viscosity of the Newtonian fluid is described by $\eta_r=1+[\eta]\phi$ with $[\eta]$ equal to $^5/_2$ for hard spheres. As was proposed by Krieger and Dougherty,[34] to fulfill the low concentration limit as well as to describe the increase of viscosity with increasing solid concentration the exponent q should be equal to $[\eta]\phi_{\text{m}}$. Conversely, the value of q derived by other authors[35,36,40] ($q=2$) does not explicitly satisfy the low concentration limit, but as was pointed out by Quemada[36], in the case of real aggregates, at low concentration the dependency of the relative viscosity on the volume fraction could be replaced by another functional form which satisfy the Einstein's limit. Here, in order to fulfill the low concentration limit as well as describe the increase of viscosity with increasing solid concentration, we chose the exponent q to be equal to $[\eta]\phi_{\text{m}}$. Using ϕ_{m} equal to 0.63 and $[\eta]$ equal to $^5/_2$ leads to the value of the exponent q equal to 1.575 which is also close to the average value of the interval mentioned earlier. In Supporting Information Figure S2, we show for comparison the relative dynamic viscosity as a function of reduced volume fraction for various values of exponent q. Since for both ϕ_{m} and q, there is a range of values possible, in what follows we will discuss influence of these values on the obtained results.

As was shown by Soos et al.,[33] when only aggregation is active, there are two possible scenarios which will lead to divergence of viscosity. On one side, when aggregation is controlled by Brownian mechanism, the divergence of viscosity is caused by volume filling with interconnection of fractal aggregates[38,44] and can be detected by calculating the value of occupied volume fraction using Eq. 24. On the other side, when aggregation is dominated by shear mechanism, the divergence of viscosity is caused by the rapid broadening of the CMD indicated by the runaway of the higher-order moments. This scenario can be detected by the evaluation of high order moment of the CMD, such as mean radius of gyration discussed later. To investigate which of these two mechanisms will be dominant in what follows a complete PBE and CFD model including the coupling of viscosity will be used.

Comparison with Experimentally Measurable Quantities

In order to validate model predictions one has to choose suitable quantities which can be compared with data measured experimentally. For example, the population of aggregates can be characterized by using static light scattering. This kind of measurement is particularly relevant because it contains information about the entire population of aggregates. In addition, sound models for optical properties of fine particles and fractal aggregates are available.[29,45] Use of these models allows the calculation of certain average quantities of the population of aggregates, such as the mean radius of gyration R_{g}, defined in dimensionless form as

$$\langle\rho_{\text{g}}\rangle=\frac{\langle R_{\text{g}}^2\rangle^{1/2}}{R_p}=\sqrt{\frac{\int_{\omega} n(\omega;\mathbf{x},t)\omega^{2(1+1/d_{\text{f}})}d\omega}{\int_{\omega} n(\omega;\mathbf{x},t)\omega^2 d\omega}} \tag{25}$$

Numerical Details

The effect of mixing on the aggregation and gelation phenomena was studied here using a tubular reactor geometry (see drawing in Figure 1) which is similar to that used by

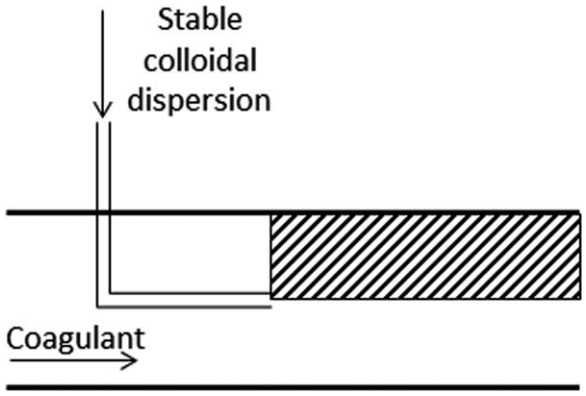

Figure 1. Drawing of the tubular jet geometry.

Due to axial symmetry all simulation were performed as 2-D assuming the striped area.

Baldyga and Orciuch[46] and Piton et al.[47] for precipitation of barium sulfate. It is constituted of an outer tube with inner diameter D^{in}_{tube} equal to 15 mm and a concentrically located thin capillary of inner diameter $D^{in}_{capillary}$ equal to 1 mm with capillary wall thickness equal to 0.25 mm. The length of the computational domain was equal to 10 times D^{in}_{tube} (=150 mm). Since the geometry is axially symmetric, the computational domain can be represented as two-dimensional. In addition, we assumed that the flow in both streams is turbulent and fully developed before they enter the reactor. Therefore, the computational domain covers only the area where mixing occurs as illustrated by shaded area in Figure 1. The computational grid contains 60 grid points in the radial direction, where 20 grid points covers the capillary, 10 grid points were used to mesh the capillary wall, and 30 grid points were used for the rest of the geometry (only $^1/_2$ of the tube diameter was used in the simulations), and 300 grid points in axial direction. Depending on the relative velocity of both streams, the produced jet can be either expanding or converging. In the case of expanding jet, the velocity of the colloidal dispersion in the capillary was equal to 10 (or 2 m/s), corresponding to $\mathrm{Re}_{capillary}=10,000(\mathrm{or}\,2000)$ while coagulant solution is fed through the outer tube with a velocity equal to 0.5 m/s corresponding to $\mathrm{Re}_{tube}=7500$. In the case of the converging jet, the velocity of the colloidal dispersion in the capillary was equal to 2 m/s while velocity of the stream containing coagulant was set to 4 m/s, corresponding to the $\mathrm{Re}_{tube}=30,000$. Assuming expanding jet, the dilution ratio between the colloidal dispersion and coagulant solution is approximately equal to 12 or 56, for 10 or 2 m/s, respectively. Conversely, in the case of converging jet, the dilution ratio is equal to 450. Since we assume that the flow of both fluids is fully developed, the velocity (axial and radial component) as well as the turbulent kinetic energy and turbulent energy dissipation rate were precalculated and used as boundary conditions at the inlet of the simulation describing mixing and aggregation.

The turbulence was described using the two-layer $k-\varepsilon$ model[48] in order to calculate all required quantities used in the PBE Eqs. 7–10, 15. The micromixing model (Eqs. 7–10) and the transport equation for the moments in environment 3 (Eq. 15) were incorporated in the CFD code ANSYS FLUENT (v12) via user-defined subroutines.[49,50] The PBE in the environment 3 was solved using the QMOMs similar to our previous work.[14] Since the environments 1 and 2 do not contain mixed components (stable dispersions of colloidal particles and coagulant solution) the value of p_1 was equal to unity in the stream of colloidal dispersion and equal to zero in the stream of coagulant solution, and vice versa for p_2, equal to zero in the stream of colloidal dispersion and equal to unity in the stream of coagulant solution. The boundary conditions for the moments were defined through the values of the kth moments in the inlet stream μ_k^* which in turn can be easily calculated from the diameter and number density of the primary particles in the colloidal dispersion. The fluxes equal to zero for all simulated scalars were used as outlet boundary conditions during the simulations. Since the aggregation process can lead to significant increase of viscosity and therefore to reduction of the degree of turbulence, in order to account for such situation the dependency of the parameter C_ϕ in the Eq. 11 on the local Reynolds number Re_1 (Eq. 12) was incorporated in our simulation.

Results and Discussion

Turbulent jet fluid dynamics and mixing

In Figures 2a–f, we show results of the simulation for colloidal solution inlet stream velocity equal to 2 m/s and coagulant solution stream with an average velocity of 0.5 m/s. As can be seen from the mean velocity profile as well as from the probability in environment 1, p_1, (see Figures 2a, b) the effect of higher inlet velocity of the colloidal dispersion stream compared to coagulant solution stream is visible only at the colloidal dispersion stream entrance and diminishes

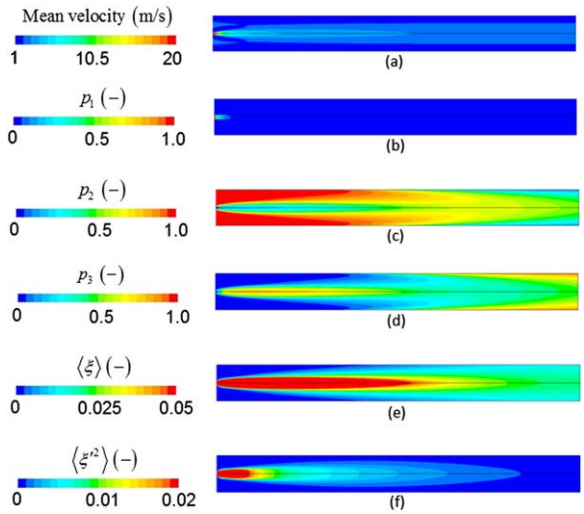

Figure 2. Profile of the mean velocity calculated for colloidal dispersion stream introduced through capillary with velocity of 2 m/s and velocity of the coagulant solution equal to 0.5 m/s (a), together with profile of probability in environment 1,2 and 3 (b–d),mean mixture fraction $\langle\xi\rangle$ (e) and mixture fraction variance $\langle\xi'^2\rangle$ (f) inside the computational domain.

In the presented simulation aggregation of 80 nm primary particles with solid volume fraction in the feed equal to 0.01 was used assuming combination of Brownian and shear aggregation mechanism including micromixing model. The d_f was equal to 1.8. [Color figure can be viewed in the online issue, which is available at wileyonlinelibrary.com.]

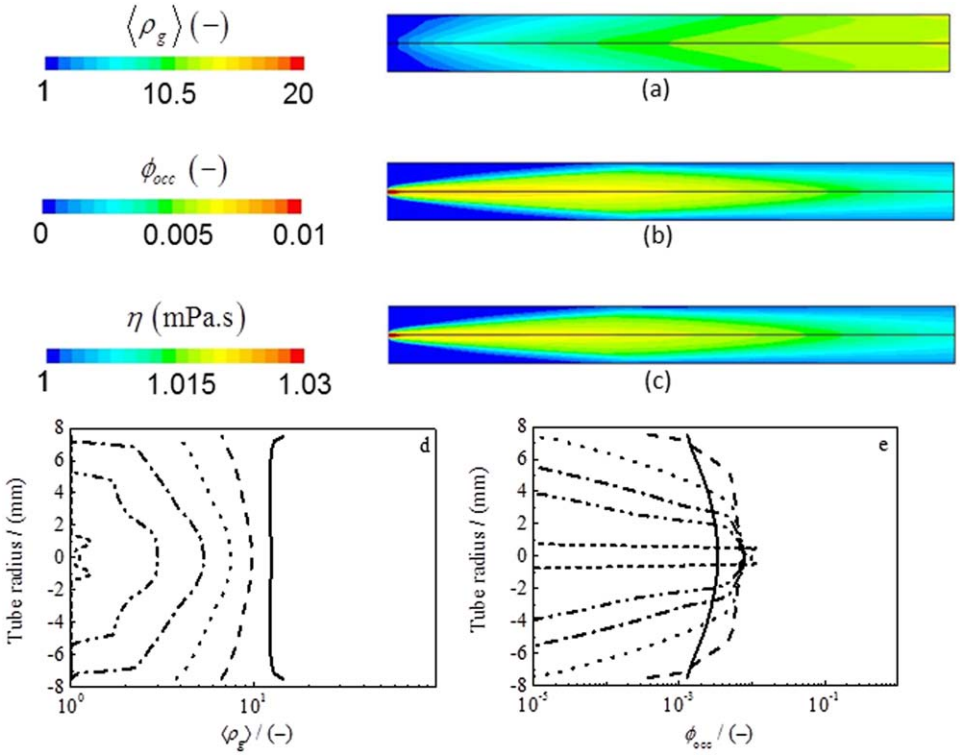

Figure 3. Contour plot of normalized mean radius of gyration (a), occupied volume fraction (b) and dynamic viscosity of the mixture (c) inside the computational domain calculated for size of primary particles equal to 80 nm and solid volume fraction in the feed equal to 0.01 using combination of Brownian and shear aggregation mechanism with micromixing model.

The d_f for presented simulation was equal to 1.8. Radial profile of $\langle \rho_g \rangle$ (d) and ϕ_{occ} (e) evaluated at various axial distances from the colloidal dispersion inlet, (short dash lined) 0 mm, (dash-double dot line) 6 mm, (dash-dot line) 15 mm, (dot line) 30 mm, (dash line) 60 mm and (solid line) 150 mm. [Color figure can be viewed in the online issue, which is available at wileyonlinelibrary.com.]

rapidly. In the case of probability in environment 2, p_2, highest values closed to one, that is, nonpremixed coagulant solutions, are located at its entrance to the computational domain and reduce gradually due to mixing (see Figure 2c). The mixing between these two streams occurs at the macroscale and microscale. To characterize macromixing, the value of the local Reynolds-averaged mixture fraction, $\langle \xi \rangle$, evaluated from Eq. 5 was used. As can be seen from Figure 2e, complete macromixing between both streams is achieved by the end of the computational domain, where $\langle \xi \rangle$ reaches its steady state value (equal to 0.0175 ± 0.0008). Complete macromixing is also supported by the same value of the volume-averaged mixture fraction, $\overline{\xi}$, equal to 0.0175 as evaluated from Eq. 3. The fact that the fluid is mixed at the macroscopic level does not imply that it is mixed also at the microscale, namely some local fluctuations around the Reynolds-averaged values, characterized by the probability/volume fraction of environment 3, can still be present. As can be seen from Figure 2d, even though macromixing is complete at the end of the computational domain values of p_3 slightly lower than one indicates that colloidal dispersion and coagulant solution streams are not perfectly micromixed.

Aggregation in turbulent jet

Since an aggregation process considered here is taking place together with mixing the real aggregation rate is evaluated as a product of the aggregation rate corresponding to fully destabilized conditions Eqs. 17 and 18, taking into consideration the local hydrodynamic characteristics, concentration and size of the particles/aggregates in the computational cell, and the value of p_3 taking into account amount of colloidal dispersion being completely mixed with coagulant and therefore promoting aggregation. As a result, the real aggregation rate becomes equal or lower compared to the maximum aggregation rate calculated for completely destabilized particles (Eqs. 17, 18). Consequently, when the concentration of colloidal particles is low enough, aggregation is slow and mixing of both colloidal dispersion and coagulant solution streams will be finished before any substantial aggregate growth occurs. From this point on, the aggregation process will be controlled by the local hydrodynamic conditions, that is, Brownian motion or shear rate, and not by micromixing anymore. Conversely, when the concentration of colloidal particles in the inlet stream is high enough, even though not perfectly mixed and therefore not fully destabilized by coagulant, aggregation proceeds quickly even before mixing is completed. It is worth noting that in extreme cases of very high solid volume fractions such fast aggregation can result in gelation in localized areas.[37] Since in the present model, we assume combined aggregation mechanisms driven by Brownian motion and shear, in the case of high colloidal particle concentrations, significant competition between both aggregation mechanisms is expected.

To demonstrate this phenomenon, the micromixing effects on the aggregation process are reported in Figures 3a–c. This figure contains the contour plots of the mean normalized radius of gyration, occupied volume fraction and effective viscosity of the mixture calculated in the case of primary

particle diameter of 80 nm and solid volume fraction of 0.01. In these simulations, combination of Brownian and shear aggregation mechanism was considered. The value of d_f used in the simulations was equal to 1.8 and was kept constant over the simulation. For completeness, the radial distribution of the mean normalized radius of gyration and occupied volume fraction plotted at various axial locations from the colloidal dispersion inlet are presented in Figures 3d, e. Under the investigated conditions, aggregation is rather slow and aggregates growth monotonically from the colloidal dispersion injection until the point when they leave the computational domain reaching size approximately 12 times that of primary particles as indicated by $\langle \rho_g \rangle$ in Figure 3a. In contrast to the observed monotonic increase of $\langle \rho_g \rangle$, the occupied volume fraction has highest values at the colloidal dispersion injection and decreases due to colloidal dispersion stream dilution (see Figure 3b). As a result, also the dynamic viscosity reaches its maximum at the point of colloidal dispersion injection and slowly decreases due to dilution of colloidal dispersion stream by coagulant solution (see Figure 3c). As shown in Figure 3d after complete mixing of both streams aggregation occurs over the whole cross-section of the channel. At this point, due to significant difference of the shear rate over the tube radius, with highest values near the wall and lowest in the tube center equal to 500 1/s and 100 1/s, respectively, aggregation rate near the wall becomes much higher compared to that at the tube axis, resulting in visible variation of the aggregate sizes along the tube radius (see Figure 3d). It is worth noting that since this study is focused on the evaluation of the onset of gelation, the breakage mechanism was not considered (we note that only aggregates above certain size become subject to hydrodynamic breakage[15,51]). Under these operating conditions, that is, used hydrodynamic conditions and selected primary particle size, a solid volume fraction equal to 0.01 is the highest possible (within the considered computational domain). By further increasing the solid volume fraction, some higher-order moments, namely the ones appearing in the definition of $\langle \rho_g \rangle$ diverge, which for this particular case occurs at the tube wall as a result of the shear aggregation mechanism before any appreciable increase of viscosity can be observed. According to Soos et al.,[33] this represents one of the two possible scenario which will lead to divergence of viscosity due to a rapid broadening of the CMD indicated in earlier mentioned case by the runaway of the higher-order moments.

Since the observed runaway occurs at the outlet of the computational domain due to divergence of $\langle \rho_g \rangle$, its surface-averaged value over the tube outlet cross-section together with the normalized dynamic viscosity is plotted versus the colloidal dispersion inlet solid volume fraction and is presented in Figure 4. As it can be seen, both plotted variables monotonically increase with increasing the colloidal dispersion solid volume fraction. Even though, the general trend for both evaluated parameters is the same, $\langle \rho_g \rangle$ reaches values which are much higher compared to that of relative viscosity. It is worth noting that due to such small increase of viscosity, a negligible effect of the aggregation process on the flow field was observed.

Since for small primary particle sizes, the relative importance of Brownian motion with respect to shear mechanism is very significant,[2,27] its stand-alone effect was further investigated. An example of such simulation calculated for primary particle diameter of 80 nm with solid volume fraction of colloidal dispersion equal to 0.3 is presented in Figures 5a–e. In comparison to the previous results, when the combination of both Brownian motion and shear aggregation was considered, it was found that even though aggregates grow to comparable sizes as in Figure 3 (with $\langle \rho_g \rangle$ around 17) now this occurs at a location much closer to colloidal dispersion injection point. In fact, if for the data presented in Figure 3, the maximum of occupied volume fraction was located at the latex inlet, for the case presented in Figure 5 the occupied volume fraction (and consequent also the dynamic viscosity) reaches its maximum at approximately 2 to 3 tube diameters from the colloidal dispersion injection point. It is worth noting that for the cases when no coupling of PBE with hydrodynamic is considered values of ϕ_{occ} between 0.5 to one are commonly considered as conditions for local gelation.[37,38,44] Since our case such coupling was considered conditions of viscosity divergence would corresponds to the point where $\phi_{occ} = \phi_m = 0.63$. Therefore, presented result corresponds to the case very close to the gelation. It can be seen that under such conditions, there is a dramatic increase of the occupied volume fraction, and therefore also viscosity, while size of formed aggregates increases only slightly. It is worth noting that as mentioned in the model description presented earlier, an increase of viscosity is fed back into the CFD code, affecting the local

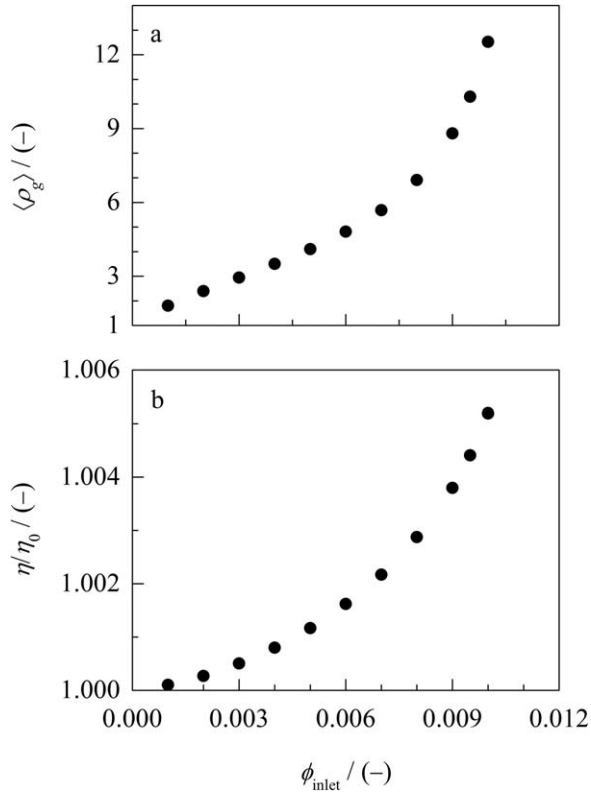

Figure 4. Evolution of mean normalized radius of gyration (a) and relative dynamic viscosity (b) at the domain outlet as a function of inlet colloidal dispersion solid volume fraction using combination of Brownian and shear aggregation mechanism.

Obtained data were calculated using size of primary particles of 80 nm with velocity of the colloidal dispersion and coagulant solution streams equal to 2 and 0.5 m/s, respectively.

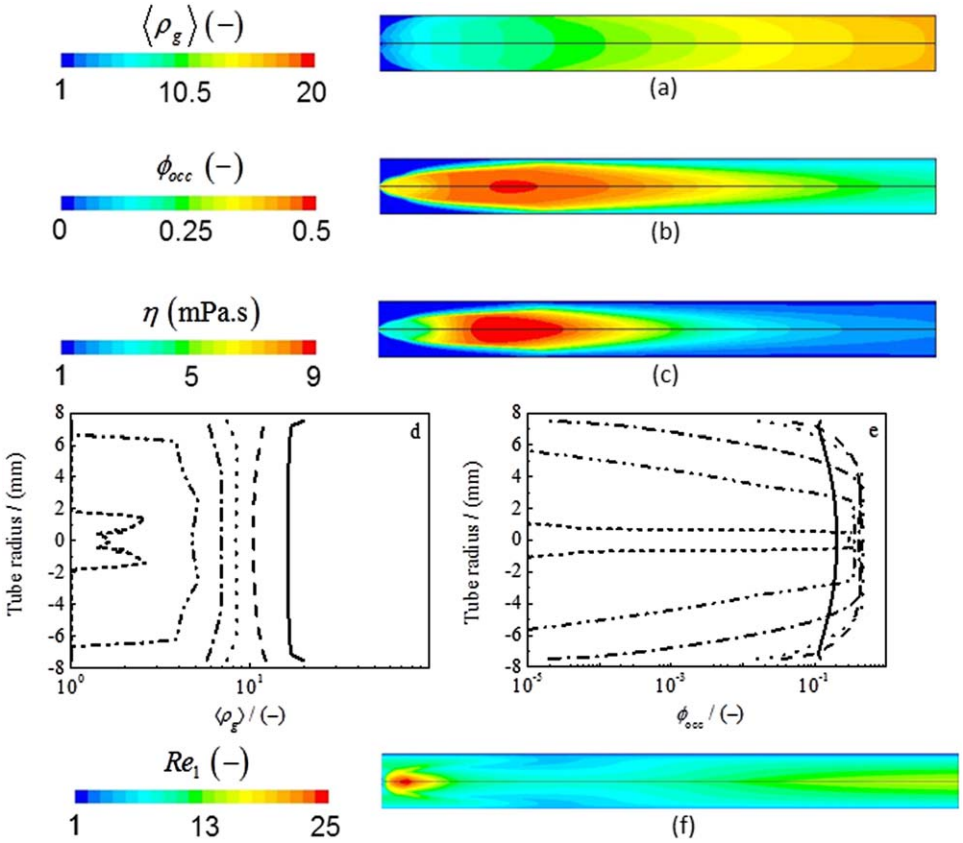

Figure 5. Profile of normalized mean radius of gyration, occupied volume fraction and dynamic viscosity of the mixture inside the computational domain calculated for size of primary particles equal to 80 nm and solid volume fraction in the feed equal to 0.3 using Brownian aggregation mechanism with micromixing model.

The d_f for presented simulation was equal to 1.8. Radial profile of $\langle \rho_g \rangle$ (d) and ϕ_{occ} (e) evaluated at various axial distances from the colloidal dispersion inlet, (short dash lined) 0 mm, (dash-double dot line) 6 mm, (dash-dot line) 15 mm, (dot line) 30 mm, (dash line) 60 mm and (solid line) 150 mm. Local Reynolds number contour plot indicating zone where increase of viscosity reduces level of turbulence (f). Velocity of the colloidal dispersion and coagulant solution streams were equal to 2 and 0.5 m/s, respectively. [Color figure can be viewed in the online issue, which is available at wileyonlinelibrary.com.]

flow field. In fact, for this particular case, a decrease of the level of turbulence, as characterized by the local Reynolds number, Re_1, was detected in correspondence to the zone of maximum viscosity (see Figures 5c, f).

To present and discuss the effect of inlet colloidal particle concentration on the aggregation process, the profiles of $\langle \rho_g \rangle$ and relative viscosity evaluated at the end of the computational domain plotted as a function of the initial colloidal dispersion solid volume fraction are shown in Figures 6a, b. Furthermore, as the maximum in ϕ_{occ} presented in Figure 5b was observed earlier than the domain outlet in Figures 6c, d are also summarized the values of $\langle \rho_g \rangle$ and of relative viscosity evaluated at the point of ϕ_{occ} maxima. It can be seen that both $\langle \rho_g \rangle$ and the normalized viscosity increase with ϕ_{Inlet}. When comparing the both these values calculated at the outlet from the computational domain (Figures 6a, b) with those evaluated when both Brownian and shear aggregation mechanisms were active (see Figures 4a, b) one can see that while the reached $\langle \rho_g \rangle$ values are for both cases rather comparable, even though a sort of plateau is observed in Figure 6a, values for viscosity are substantially higher when Brownian motion is acting alone. This difference is even more pronounced when comparing viscosities of the fluid evaluated near the point of ϕ_{occ} maxima. This indicates that in the case when aggregation is driven by Brownian motion alone the point when viscosity diverges is reached first which is phenomenon similar to that occurring under static conditions when dramatic increase of viscosity with finite size of formed aggregates was documented around the gel point.[37,38,44] When considering profile of $\langle \rho_g \rangle$ the plateau observed at high inlet solid volume fractions corresponds to the reduced action of the aggregation mechanism (i.e., Brownian motion) with the increase of an aggregate sizes. In particular, for primary particles with diameter of about 80 nm, the reached maxima correspond to aggregates of size around 1 micron, at which Brownian motion becomes nearly negligible and aggregates do not further grow at a significant rate, resulting in almost constant $\langle \rho_g \rangle$ for ϕ_{Inlet} ranging from 0.15 to 0.3 (see Figure 6a). In the case of observed profile of $\langle \rho_g \rangle$ evaluated at the point of ϕ_{occ} maxima presented in Figure 6c observed maxima followed by slow decay is related to the shorter distance of ϕ_{occ} maxima from the latex feed, and therefore effectively shorter time of the aggregation. Since only Brownian aggregation mechanism was considered if shear aggregation would be present, it would take over resulting in much larger aggregate sizes. However, as discussed earlier before this happens gelation will occur due to viscosity divergence caused by volume filling with interconnection of fractal aggregates.[33,38,44] Therefore, these two mentioned situations represent the two

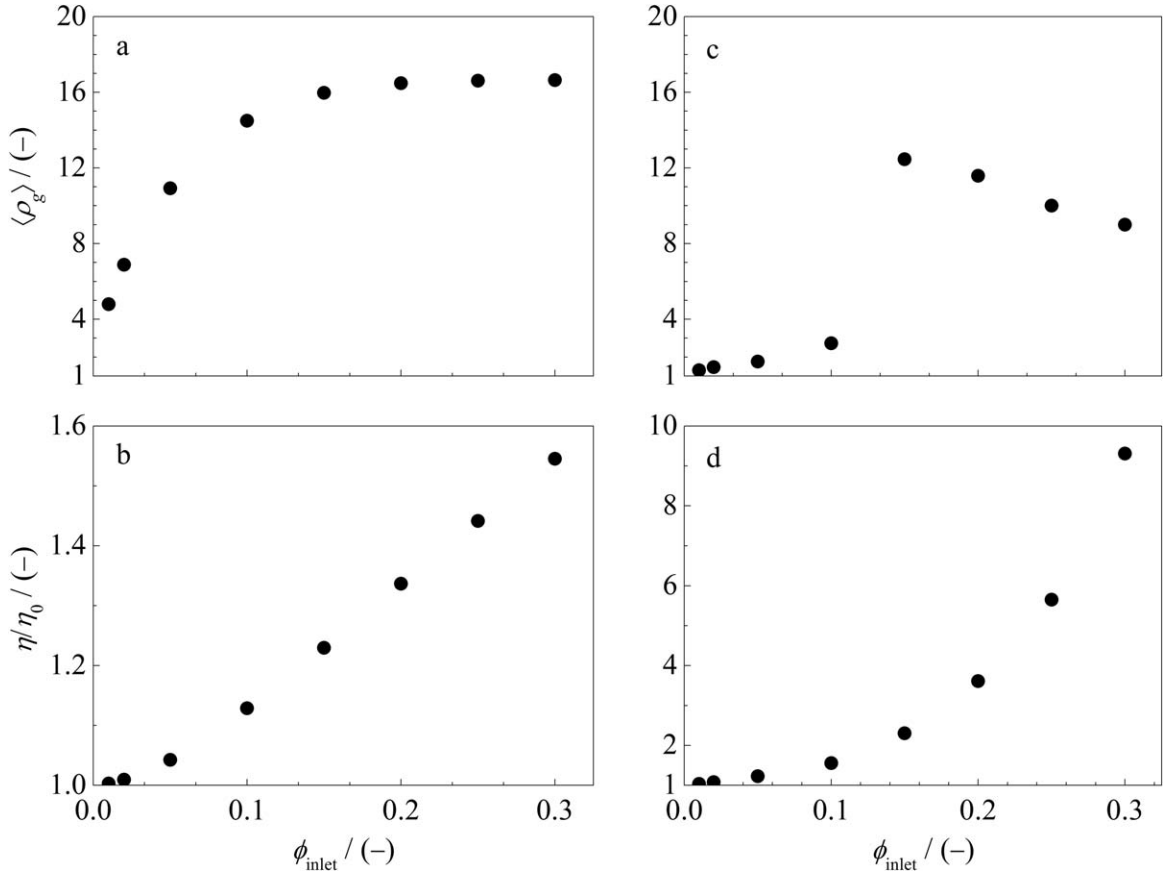

Figure 6. Evolution of mean normalized radius of gyration (a, c) and relative dynamic viscosity (b, d) as a function of inlet colloidal dispersion solid volume fraction using Brownian aggregation mechanism only.

Left column was evaluated at the end of the computational domain while right column was calculated at the point where ϕ_{occ} reaches its maximum. Obtained data were calculated using diameter of primary particles of 80 nm with velocity of the colloidal dispersion and coagulant solution streams equal to 2 and 0.5 m/s, respectively.

limits on how gelation due to mixing and simultaneous aggregation could occur. Obviously, this would have strong implication on the final size, shape and internal structure of formed aggregates.

Combining now this information with the evolution of viscosity as a function of solid volume fraction presented in Supporting Information Figure S2, we can conclude that for the high value of the ϕ_{Inlet} by increasing the value of the parameter q in Eq. 23, from 1.575 used in the simulations to 2.0, will lead to the increase of mixture viscosity approximately two times compared to the presented results. Conversely, reducing the value of parameter q to 1.3 will lead to the reduction of the mixture viscosity again approximately two times with respect to the presented results. In the case of lower value of the ϕ_{Inlet}, no significant difference in viscosity will be observed for any value of the parameter q from the aforementioned interval, due to relatively small aggregates growth. Another parameter in the functional form of viscosity Eq. 23, is the maximum packing volume fraction ϕ_m. As it was mentioned earlier, other values covering the range from 0.5 to 0.74 are possible. It is obvious that reduction of the value ϕ_m will lead to the shift of the point when viscosity diverges to the smaller values of ϕ_{Inlet} approximately by 20%. On the contrary, when we increase the value of the ϕ_m, we shift the point of viscosity divergence approximately about the same value towards larger values of ϕ_{Inlet}.

Gelation regimes in process parameter space

When considering results presented so far parameters which would affect the process of aggregation are the size of primary particles, their solid volume fraction in the inlet stream and d_f of the formed aggregates. The summary of simulations performed by varying all these parameters are presented in Figures 7a–c in the form of process parameter space using two different d_f equal to 1.8 and 2.2, respectively. For a more general picture results for three different flow conditions are included, that is, expanding jet using velocities of colloidal dispersion stream equal to 2 and 10 m/s and coagulant solution stream with velocity of 0.5 m/s (see Figures 7a, b), and converging jets using velocity of colloidal dispersion stream equal to 2 m/s and coagulant solution stream with velocity equal to 4 m/s (see Figure 7c). It is worth noting that all points presented in the Figures 7a–c corresponds to the converged simulation. Two borderlines were identified. The first one corresponds to the situation where the runaway of $\langle \rho_g \rangle$ was observed before detecting the gelation due to combined action of Brownian and shear aggregation mechanisms. The second boundary corresponds to the situation where gelation due to viscosity divergence with Brownian motion acting alone was observed. As a result of these simulations, the process parameter space is split into three distinct regions. In the first region (denoted I. in Figure 7), corresponding to rather large primary particles combined with low solid volume fraction in the inlet stream,

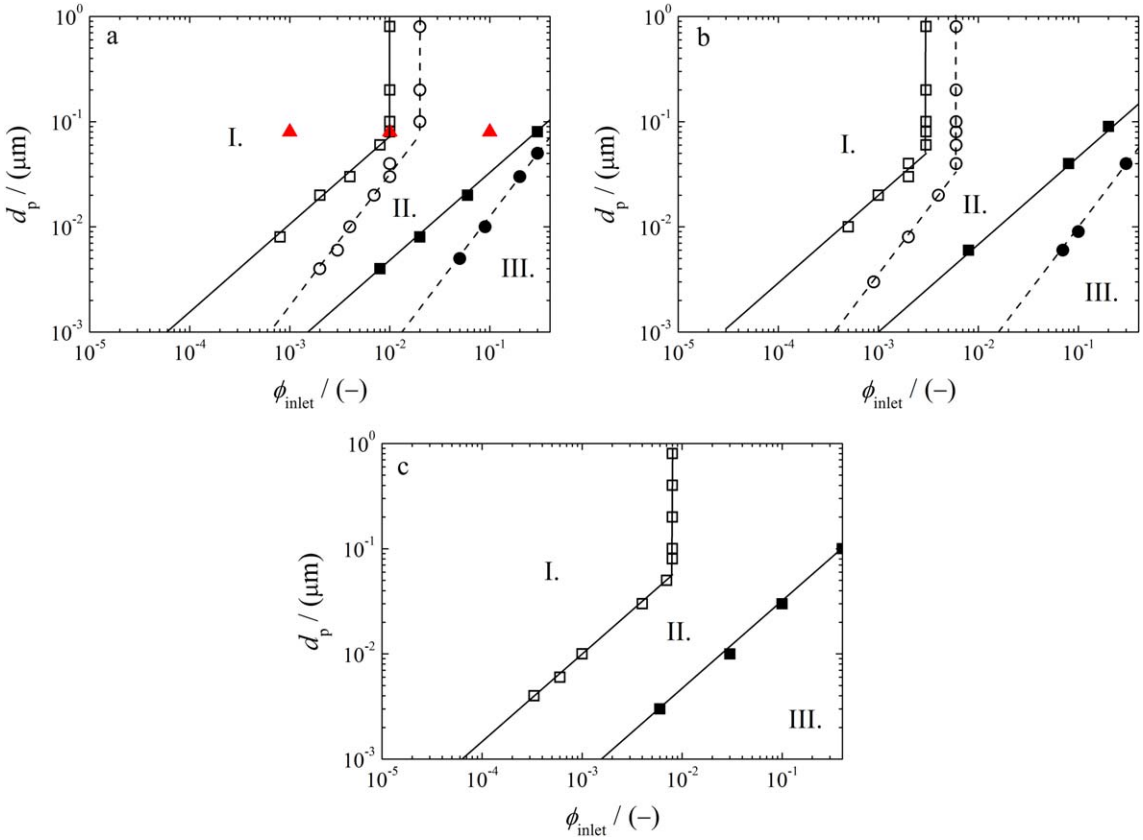

Figure 7. Process parameter space of particle diameter as a function of inlet solid volume fraction for aggregation under turbulent conditions calculated in tubular jet geometry for d_f equal to 1.8 (square) and 2.2 (circle) and three different flow configurations.

(a) average velocity of colloidal dispersion and coagulant solution streams equal to 2 and 0.5 m/s, respectively, (b) average velocity of colloidal dispersion and coagulant solution streams equal to 10 and 0.5 m/s, respectively, (c) average velocity of colloidal dispersion and coagulant solution streams equal to 2 and 4 m/s, respectively. Open symbols corresponds to simulation performed with combination of Brownian and shear aggregation mechanism while solid symbols represent simulations with only Brownian aggregation mechanism active. Triangles represent the conditions used during an aggregation experiment in the stirred tank. [Color figure can be viewed in the online issue, which is available at wileyonlinelibrary.com.]

neither divergence of viscosity nor runaway of $\langle \rho_g \rangle$ was observed before complete macromixing of the two streams. The second region (denoted II. in Figure 7) corresponds to the moderate primary particle size combined with intermediate solid volume fraction, where runaway of $\langle \rho_g \rangle$ is occurring before volume filling, that is, viscosity divergence, due to combined action of Brownian and shear aggregation mechanisms. This occurs before complete macromixing between the two streams. The third region (denoted III. in Figure 7) corresponds to very small primary particles combined with very high solid volume fraction. For such conditions gelation can be achieved by the Brownian motion acting alone, even before the shear aggregation mechanism can become active.

When comparing the position of the borderlines calculated for d_f equal to 1.8 and 2.2, it seems that they are shifted toward lower solid volume fraction or higher primary particles when d_f is decreased. Such shift is related to the fact that having lower d_f results in the formation of larger, even though sparse aggregates so volume filling or runaway of $\langle \rho_g \rangle$ is reached earlier. Furthermore, when considering the boundary between region I and II, in the region of small particles, it follows a power law which is a function of the used d_f. Conversely, above certain primary particle size no dependency on the primary particle size can be observed, even though still being function of d_f. The same power law dependency between the demarcation line of regions I and II with that observed for regions II and III, indicates that both of them are controlled by the same mechanism, which in this particular case is due to Brownian motion acting alone. By detailed analysis of the gelation time for the case of pure Brownian mechanism (as shown by Bremer et al.[52] and Sefcik et al.[53]), it was found that this depends on both primary particle size as well as solid volume fraction in the inlet stream according to

$$t_g^{\text{Brownian}} \propto \frac{d_p^3}{\phi_{inlet}^{3/(3-d_f)}} \tag{26}$$

When assuming that characteristic time for gelation would be constant according to this equation, data plotted in Figures 7a–c should scale with a power equal to $(3-d_f)^{-1}$. In fact, as can be seen all data below approximately 80 nm follow closely this scaling, which supports the assumption about comparable gelation time. This clearly indicates that despite turbulent conditions, a critical size of primary particles below which the effect of Brownian motion is the controlling mechanism exists. In contrast, above certain size values aggregation is controlled by shear aggregation. In

such cases, the characteristic time of gelation is only a function of applied shear rate and solid volume fraction but does not depend on the primary particle size; a trend clearly evidenced by the data reported in Figures 7a–c.

When velocity of the colloidal dispersion stream is increased to 10 m/s (see Figure 7b) both boundaries between region I and II for both d_f values are shifted toward lower values of the solid volume fraction. The reason for such behavior is the lower dilution ratio between colloidal dispersion and coagulant solution, resulting in large concentrations of primary particles in the final mixture, and therefore, faster aggregation.

The last scenario which we would like to address is the case of a tubular reactor with converging jet, where the colloidal dispersion stream velocity is smaller than that containing the coagulant. An example of the space evolution of probability in environment 1–3, mixture fraction mean and variance, $\langle \rho_g \rangle$, ϕ_{occ} and dynamic viscosity is presented in Supporting Information Figure S3a–e and S4a–c. Since the flow rate of the stream containing primary particles is significantly smaller than that of coagulant (dilution ration 450), the effect of micromixing is almost negligible. Conversely, as the velocity of the colloidal dispersion stream is smaller than coagulant solution stream, there will be very small radial dispersion of particles/aggregates resulting in faster aggregation rate, and therefore, also large aggregate sizes in the tube center (see evolution of $\langle \rho_g \rangle$ and ϕ_{occ} in Supporting Information Figures S4a,b, and S5). As a consequence, the boundary between region I and II does not represent the limit of complete macromixing over the whole tube diameter. Instead they represent the limiting case before runaway occurrence, however, for these particular conditions due to low radial mixing of colloidal dispersion stream along the reactor axis. Due to higher concentration of particles which are not well mixed in radial direction the vertical boundary between region I and II, corresponding to shear aggregation mechanism controlling the process, is shifted toward small values of ϕ_{inlet} with respect to the expanding jet condition. In contrast, for the case when Brownian aggregation mechanism acing alone the boundary between region II and III do not move with respect to expanding jet conditions. Since in both aforementioned conditions, the zone where viscosity divergence occurs is located in the center of the flow near the colloidal dispersion injection point very similar results were obtained.

Since the breakage was not considered in this work, let us now discuss its significance to the presented results. As explained earlier, the region III presented in Figure 7 corresponds to the situation where gelation due to viscosity divergence was observed. This means that under these conditions, the occupied volume fraction calculated from PBE increases substantially reaching values comparable to ϕ_m. As can be seen from Eq. 23, ϕ_m represents the solid volume fraction where the viscosity of the particle dispersion diverges which is in agreement with the presented results. In contrast size of formed aggregates is at this point very small approximately 1 micron. As it was shown in our previous works using comparable values of the shear rate,[6,15,17,51] this size is substantially lower than the limit when breakage becomes significant, hence omitting breakage would not affect the presented results. In the case of region II, where runaway of $\langle \rho_g \rangle$ was observed, aggregates could grow large enough to be affected by the breakage. However, due to their fast growth (runaway) increase of the size controlled by the shear aggregation kernel (Eq. 18) would be so fast that the proper modeling combined with proper description of the hydrodynamic becomes very challenging. Since the main goal of this work was to describe the early stage of the aggregation process in combination with the mixing such modeling is out of the scope of this work. Last is the region I where mixing is so fast that size of aggregates increases only little compared to the primary particles size so the effect of breakage would not affect the presented results. To model the whole process an approach presented previously by Marchisio et al.[14,54] could be used. In this case, the final size of formed aggregates would be controlled by the dynamic equilibrium between aggregation and breakage which is a function of the distribution of the shear rate in the applied vessel.

Interpretation of aggregation experiment in stirred tank

The data obtained from the aforementioned simulations were in what follows used to interpret aggregation experiments performed in the stirred tank when latex with various solid volume fractions was fed into the salt solution presented in the vessel. A setup used by Vaccaro et al.[8] was used to performed these aggregation experiments. It is based on a stirred tank equipped with two Rushton impellers filled with 6 L of a coagulant ($Al(NO_3)_3$) solution. To ensure fast mixing stable dispersion of polystyrene nanoparticles with diameter of 80 nm was injected through a capillary with diameter of 1.5 mm whose outlet was located at the point of maximal radial jet generated by the bottom impeller. It is worth noting that to ensure complete destabilization of primary particles the salt concentration was approximately 20 times higher than the critical coagulation concentration. To keep experimental conditions qualitatively comparable to the conditions used in the simulations impeller stirring speed was set to 100 rpm, resulting in a coagulant solution stream velocity of 0.47 m/s, while the colloidal dispersion injection flow rate was set to 160 mL/min resulting in a linear velocity in the capillary equal to 1.5 m/s. Used conditions in terms of colloidal dispersion solid volume fraction and primary particle diameter are plotted as triangles in Figure 7a. Corresponding pictures of the mixing process together with SEM images of formed aggregates are presented in Figures 8a–c. As can be seen from Figure 8a1, when colloidal dispersion with solid volume fraction equal to 1×10^{-3} was injected in the reactor slow aggregation allows complete mixing of coagulant with primary particles corresponding to the region I from Figure 7a. As a result homogeneously mixed particles aggregate with rate dependent on the local values of the shear rate present in the stirred tank. When their size becomes large enough they become broken by the hydrodynamic stress exposed on them by fluid flow leading to formation of aggregates with round shape having very compact structure (Figure 8a2).

A different situation was observed when the solid volume fraction was increased to 1×10^{-2}. For this concentration, the aggregation process was already fast enough compared to mixing and formation of large aggregates approximately 5 to 10 cm from the injection point was observed (see Figure 8b1). When considering the process parameter space discussed earlier (see Figure 7a), this conditions corresponds to the region II where runaway of aggregate size was detected. Effect of micromixing on the shape of formed aggregates was further supported by SEM pictures where more irregular aggregates were observed (see Figure 8b2).

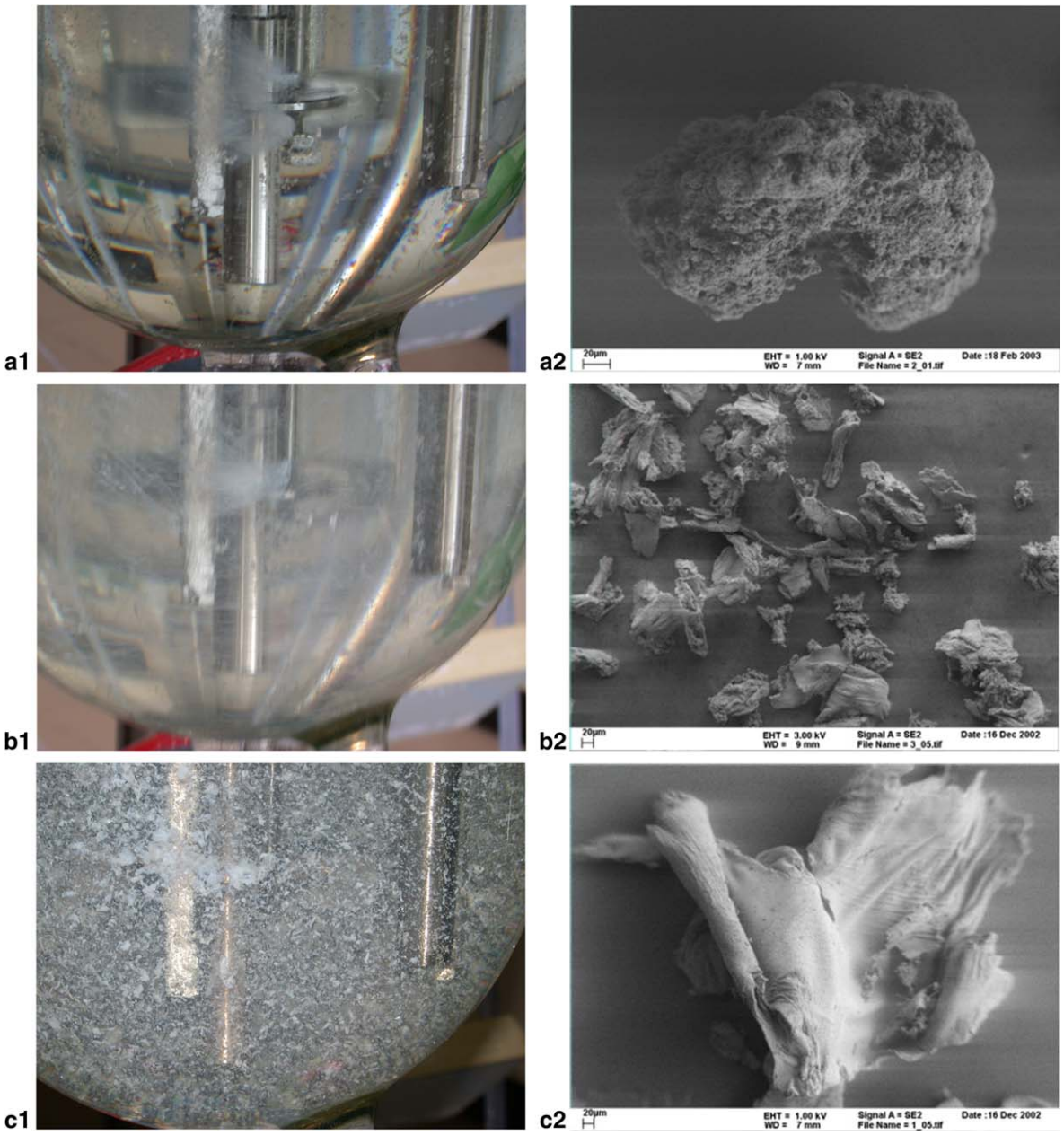

Figure 8. Comparison of various feeding conditions using stirred tank with volume of 6 L, $D_{impeller}$ equal to 9 cm and impeller rotation speed of 100 rpm.

Latex solution containing 80-nm polystyrene particles was injected through 1.5 mm capillary into the concentrated solution of coagulant ($Al(NO_3)_3$). Left column represents pictures of the mixing behavior closed to latex injection point, Right column corresponds to the SEM pictures of formed final aggregates. (a1, a2) corresponds to $\phi_{inlet} = 1 \times 10^{-3}$, (b1, b2) $\phi_{inlet} = 1 \times 10^{-2}$, (c1, c2) $\phi_{inlet} = 1 \times 10^{-1}$. [Color figure can be viewed in the online issue, which is available at wileyonlinelibrary.com.]

The last condition investigated experimentally corresponds to the particle solid volume fraction equal to 1×10^{-1}. For such high particle concentration, clearly visible pieces of gel were formed at the point of colloidal dispersion injection (see Figure 8c1). In fact, when considering the process parameter space presented in Figure 7, this point would be very close to the boundary between region II and III where local gelation is due to Brownian aggregation mechanism acting alone. Strong effect of micromixing on the structure of formed aggregates is clearly visible also on SEM picture presented in Figure 8c2. Under these conditions, formed aggregates have sheet like shape with large ratio of diameter to thickness. This can be explained by the local gelation of primary particles occurring on the length scale of several primary particles, corresponding to the diffusion path of a coagulant. Due to the increase of local viscosity, the formed gel keeps its longitudinal integrity resulting in sheet-like structures.

Conclusions

In this work, effect of mixing on the process of aggregation and gelation was studied numerically by using a combination of CFD and population balance models. The effect of mixing on aggregation was modeled by a presumed PDF method. Since formed aggregates could change the surrounding flow, an effective viscosity of the mixture evaluated from PBE was used to modify the fluid viscosity to calculate

the flow field. The obtained results are summarized in the form of parameter space of the solid volume fraction and the primary particle diameter and three distinct regions were identified. In the first region, covering large primary particle size with low solid volume fraction, due to slow aggregation micromixing does not play any significant role. In the second region, corresponding to moderate particle size and moderate solid volume fraction, local gelation could occur due to shear aggregation characterized by the runaway of higher-order moments of the PSD before viscosity divergence. In the last region, the available space is filled as a result of viscosity increase before higher-order moments of the calculated PSD runs away. Under such conditions, the aggregation of small primary particles with high solid volume fraction is controlled solely by Brownian motion. Obtained results are in good agreement with experimental data obtained from gelation experiment of concentrated nanoparticle suspensions into coagulant solution.

Acknowledgments

Authors would like to thank to Prof. Massimo Morbidelli for valuable comments and suggestions. This work was financially supported by Swiss National Science Foundation (Grant 200020_147137/1).

Notation

A_i = parameter of the micromixing model used to evaluate C_ϕ, −
C_μ = parameter of the k−ε model, −
C_ϕ = parameter of the micromixing model, -
d_f = fractal dimension, –
d_p = primary particle diameter, m
D_i = diffusion coefficient of the i-th aggregate, m^2/s
D_t = turbulent diffusivity, m^2/s
$D^{in}_{capillary}$ = inner diameter of the capillary, m
D^{in}_{tube} = inner diameter of the tube, m
G = shear rate, 1/s
k = turbulent kinetic energy, m^2/s^2
k_B = Boltzmann constant, J/K
k_g = prefactor of the fractal scaling, −
K^A = aggregation kernel, m^3/s
$K^{Brownian}$ = Brownian aggregation kernel, m^3/s
K^{Shear} = shear aggregation kernel, m^3/s
n = number concentration of aggregates with mass ω
N = number of nodes of the quadrature approximation, −
N_e = total number of modes/environments, −
p_n = probability of the mode n or the volume fraction of environment n, −
R_i = radius of the i-th aggregate, m
R_p = primary particle radius, m
$Re_{capillary}$ = Reynolds number in the latex feeding capillary, −
Re_l = local Reynolds number $(=k/\sqrt{\varepsilon v})$, −
Re_{tube} = Reynolds number in the tube, −
q = scaling exponent in the apparent viscosity equation, −
Q_i = flow rate in the stream I, m^3/s
Sc_t = turbulent Schmidt number
T = absolute temperature, K
$\langle u_i \rangle$ = i-th component of the Reynolds-averaged fluid velocity, m/s
$w_{i,n}$ = i-th weight of the quadratic approximation in mode/environment n, −
W = Fuchs stability ratio, −
$\mathbf{x}$ = spatial coordinate vector
x_i = i-th spatial coordinate, m
t = time, s
t_g = gelation time, s

Greek letters

α_A = efficiency in the shear aggregation kernel, −
ε = turbulent energy dissipation rate, m^2/s^3
ϕ_{eff} = effective volume fraction of the particles in the mixture, −
ϕ_{inlet} = volume fraction of the particles in the latex inlet stream, −
ϕ_m = maximum packing volume fraction, −
ϕ_{occ} = occupied volume fraction, −
γ = micromixing parameter
η = dynamic viscosity, Pa.s
η_0 = dynamic viscosity of a pure liquid, Pa.s
μ^k = k-th moment of the PSD, −
μ^k_n = k-th moment of the quadratic approximation in mode/environment n, −
ν = kinetic liquid viscosity, m^2/s
$\langle \rho_g \rangle$ = dimensionless radius of gyration, −
ω = dimensionless mass of an aggregate, −
$\omega_{i,n}$ = i-th abscissa of the quadratic approximation in mode/environment n, −
ξ_n = mixture fraction corresponding to mode n
$\bar{\xi}$ = mixture fraction mean, −
$\langle \xi \rangle$ = volume-averaged mixture fraction, −
$\langle \xi'^2 \rangle$ = mixture fraction variance, −
ψ = is the composition vector

Literature Cited

1. Israelachvili JN. *Intermolecular and Surface Forces, 3rd ed.* London: Academic Press, 2011.
2. Russel WB, Saville DA, Schowalter WR. Colloidal Dispersions. Cambridge: Cambridge University Press, 1989.
3. Lin M, Lindsay HM, Weitz DA, Ball RC, Klein R, Meakin P. Universal diffusion-limited aggregation. *J Phys-Condens Mater*. 1990; 2(13):3093–3113.
4. Lin M, Lindsay HM, Weitz DA, Klein R, Ball RC, Meakin P. Universal reaction-limited aggregation. *Phys Rev A*. 1990;41(4):2005–2020.
5. Lin MY, Lindsay HM, Weitz DA, Ball RC, Klein R, Meakin P. Universality in colloid aggregation. *Nature*. 1989;339:360–362.
6. Soos M, Moussa A, Ehrl L, Sefcik J, Wu H, Morbidelli M. Effect of shear rate on aggregate size and morphology investigated under turbulent conditions in stirred tank. *J Colloid Interface Sci*. 2008;319 577—589.
7. Moussa AS, Soos M, Sefcik J, Morbidelli M. Effect of the solid volume fraction on the aggregation and breakage of colloidal suspensions in batch and continuous stirred tank. *Langmuir*. 2007;23:1664–1673.
8. Vaccaro A, Sefcik J, Wu H, Morbidelli M, Bobet J, Fringant C. Aggregation of concentrated polymer latex in stirred vessels. *AIChE J*. 2006;52:2742–2756.
9. Marchisio DL, Barresi AA, Fox RO. Simulation of turbulent precipitation in a semi-batch Taylor-Couette reactor using CFD. *AIChE J*. 2001;47(3):664–676.
10. Marchisio DL, Fox RO, Barresi AA, Garbero M, Baldi G. On the simulation of turbulent precipitation in a tubular reactor via Computational Fluid Dynamics (CFD). *Trans IChenE Part A*. 2001;79:998–1004.
11. Marchisio DL, Omegna F, Barresi AA, Bowen P. Effect of mixing and other operating parameters in sol-gel processes. *Ind Eng Chem Res*. 2008;47(19):7202–7210.
12. Gavi E, Marchisio DL, Barresi AA, Olsen MG, Fox RO. Turbulent precipitation in micromixers: CFD simulation and flow field validation. *Chem Eng Res Des*. 2010;88(9A):1182–1193.
13. Liu Y, Cheng CY, Prud'homme RK, Fox RO. Mixing in a multi-inlet vortex mixer (MIVM) for flash nano-precipitation. *Chem Eng Sci*. 2008;63(11):2829–2842.
14. Marchisio DL, Soos M, Sefcik J, Morbidelli M. Role of turbulent shear distribution in aggregation and breakage processes. *AIChE J*. 2006;52:158–173.
15. Ehrl L, Soos M, Morbidelli M. Dependence of aggregate strength, structure, and light scattering properties on primary particle size under turbulent conditions in stirred tank. *Langmuir*. 2008;24:3070–3081.
16. Ehrl L, Soos M, Bäbler MU, Morbidelli M. Dependence of initial cluster aggregation kinetics on shear rate for particles of different sizes under turbulence. *AIChE J*. 2009;55(12):3076–3087.
17. Bäbler MU, Moussa AS, Soos M, Morbidelli M. Structure and kinetics of shear aggregation in turbulent flows. I. Early stage of aggregation. *Langmuir*. 2010;26(16):13142–13152.
18. Fox FO. *Computational Models for Turbulent Reacting Flows*. Cambridge: Cambridge University Press, 2003.
19. Liu Y, Fox FO. CFD predictions for chemical processing in a confined impinging-jets reactor. *AIChE J*. 2006;52:731–744.

20. Ramkrishna D. *Population Balances*. San Diego: Academic Press, 2000.
21. Marchisio DL, Pikturna JT, Fox RO, Vigil RD, Barresi AA. Quadrature method of moments for population-balance equations. *AIChE J*. 2003;49(5):1266–1276.
22. Marchisio DL, Vigil RD, Fox RO. Quadrature method of moments for aggregation-breakage processes. *J Colloid Interface Sci*. 2003; 258(2):322–334.
23. Hulburt HM, Katz S. Some problems in particle technology. *Chem Eng Sci*. 1964;19:555–574.
24. McGraw R. Description of aerosol dynamics by the quadrature method of moments. *Aerosol Sci Technol*. 1997;27:255–267.
25. Gordon RG. Error bounds in equilibrium statistical mechanics. *J Math Phys*. 1968;9:655–667.
26. Melis S, Verduyn M, Storti G, Morbidelli M, Baldyga J. Effect of fluid motion on the aggregation of small particles subject to interaction forces. *AIChE J*. 1999;45(7):1383–1393.
27. Elimelech M, Gregory J, Jia X, Williams RA. *Particle Deposition and Aggregation, Measurement, Modelling and Simulation*. Woburn: Butterworth-Heinemann, 1995.
28. Saffman P, Turner J. On the collision of drops in turbulent clouds. *J Fluid Mech*. 1956;1:16–30.
29. Sorensen CM. Light scattering by fractal aggregates: A review. *Aerosol Sci Technol*. 2001;35:648–687.
30. Lattuada M, Wu H, Morbidelli M. A simple model for the structure of fractal aggregates. *J Colloid Interface Sci*. 2003;268:106–120.
31. Lattuada M, Wu H, Morbidelli M. Hydrodynamic radius of fractal clusters. *J Colloid Interface Sci*. 2003;268:96–105.
32. Waldner MH, Sefcik J, Soos M, Morbidelli M. Initial growth kinetics of aggregates in turbulent coagulator. *Powder Tech*. 2005; 156:226–234.
33. Soos M, Sefcik J, Morbidelli M. Master curves for shear aggregation: effects of cluster structure and polydispersity. *Ind Eng Chem Res*. 2007;46:1709–1720.
34. Krieger IM, Dougherty TJ. A mechanism for non-Newtonian flow in suspensions of rigid spheres. *Trans Soc Rheol*. 1959;3:137–152.
35. Quemada D. Rheology of concentrated disperse systems. I. Minimum energy dissipation principle and viscosity-concentration relationship. *Rheol Acta*. 1977;16:82–94.
36. Quemada D. Rheological modelling of complex fluids. I. The concept of effective volume fraction revisited. *Eur Phys J AP*. 1998;1:119–127.
37. Sandkühler P, Sefcik J, Morbidelli M. Kinetics of aggregation and gel formation in concentrated polystyrene colloids. *J Phys Chem B*. 2004;108(52):20105–20121.
38. Sandkühler P, Sefcik J, Morbidelli M. Scaling of the kinetics of slow aggregation and gel formation for a fluorinated polymer colloid. *Langmuir*. 2005;21:2062–2077.
39. McGeary RK. Mechanical packing of spherical particles. *J Am Ceram Soc*. 1961;44:513–522.
40. Maron SH, Pierce PE. Application of Ree-Eyring generalized flow theory to suspensions of spherical particles. *J Colloid Sci*. 1956;11: 80–95.
41. Papir YS, Krieger IM. Rheological studies on dispersions of uniform colloidal spheres: II. Dispersions in nonaqueous media. *J Colloid Interface Sci*. 1970;34:126–130.
42. Stickel JJ, Powell RL. Fluid mechanics and rheology of dense suspensions. *Ann Rev Fluid Mech*. 2005;37:129–149.
43. Einstein A. *Investigations on the Theory of the Brownian Movement*. New York: Dover, 1956.
44. Sandkühler P, Sefcik J, Morbidelli M. Kinetics of gel formation in dilute dispersions with strong attractive particle interactions. *Adv Colloid Interface Sci*. 2004;108:133–143.
45. Soos M, Lattuada M, Sefcik J, Morbidelli M. Interpretation of light scattering and turbidity measurements in aggregated systems: effect of intra-cluster multiple-light scattering. *J Phys Chem B*. 2009;113: 14962–14970.
46. Baldyga J, Orciuch W. Barium sulphate precipitation in a pipe - an experimental study and CFD modelling. *Chem Eng Sci*. 2001;56(7): 2435–2444.
47. Piton D, Fox RO, Marcant B. Simulation of fine particle formation by precipitation using computational fluid dynamics. *Can J Chem Eng*. 2000;78:983–993.
48. Chen HC, Patel VC. Near-wall turbulence models for complex flows including separation. *AIAA J*. 1988;26:509–529.
49. ANSYS, I. *ANSYS FLUENT 12.1 User's Guide*. Canonsburg PA, USA, 2009.
50. ANSYS, I., *ANSYS FLUENT 12.1 UDF User's Guide*. Canonsburg PA, USA, 2009.
51. Soos M, Ehrl L, Bäbler MU, Morbidelli M. Aggregate breakup in a contracting nozzle. *Langmuir*. 2010;26:10–18.
52. Bremer LGB, Walstra P, van Vliet T. Estimation of the aggregation time of various colloidal systems. *Colloids Surf A*. 1995;99:121–127.
53. Sefcik J, Soos M, Vaccaro A, Morbidelli M. Effects of mixing on aggregation and gelation of nanoparticles in turbulent flows. *Chem Eng Proc*. 2006;45:936–943.
54. Marchisio DL, Soos M, Sefcik J, Morbidelli M, Barresi AA, Baldi G. Effect of fluid dynamics on particle size distribution in particulate processes. *Chem Eng Technol*. 2006;29:191–199.

Manuscript received Jan. 31, 2013, revision received July 12, 2013, and final revision received Oct. 13, 2013.